Unconventional Superconducting Quantum Criticality in Monolayer WTe₂

Tiancheng Song¹, Yanyu Jia¹, Guo Yu^{1,2}, Yue Tang¹, Pengjie Wang¹, Ratnadwip Singha³, Xin Gui³, Ayelet J. Uzan¹, Michael Onyszczak¹, Kenji Watanabe⁴, Takashi Taniguchi⁵, Robert J. Cava³, Leslie M. Schoop³, N. P. Ong¹, Sanfeng Wu^{1*}

¹Department of Physics, Princeton University, Princeton, New Jersey 08544, USA.

²Department of Electrical and Computer Engineering, Princeton University, Princeton, New Jersey 08544, USA.

 ³Department of Chemistry, Princeton University, Princeton, New Jersey 08544, USA.
 ⁴Research Center for Functional Materials, National Institute for Materials Science, 1-1 Namiki, Tsukuba 305-0044, Japan.

⁵International Center for Materials Nanoarchitectonics, National Institute for Materials Science, 1-1 Namiki, Tsukuba 305-0044, Japan.

*Correspondence to: <u>sanfengw@princeton.edu</u>

Abstract

The superconductor to insulator or metal transition in two dimensions (2D) provides a valuable platform for studying continuous quantum phase transitions (OPTs) and critical phenomena^{1,2}. Distinct theoretical models, including both fermionic and bosonic localization scenarios¹⁻³, have been developed, but many questions remain unsettled despite decades of research^{1,2}. Extending Nernst experiments down to millikelvin temperatures, we uncover anomalous quantum fluctuations and identify an unconventional superconducting quantum critical point (QCP) in a gate-tuned excitonic quantum spin Hall insulator (QSHI)⁴⁻¹¹, the monolayer tungsten ditelluride (WTe2). The observed vortex Nernst effect reveals singular superconducting fluctuations in the resistive normal state induced by magnetic fields or temperature, even well above the transition. Near the doping-induced QCP, the Nernst signal driven by quantum fluctuations is exceptionally large in the millikelvin regime, with a coefficient of ~ 4,100 µV/KT at zero magnetic field, an indication of the proliferation of vortices. Surprisingly, the Nernst signal abruptly disappears when the doping falls below the critical value, in striking conflict with conventional expectations. This series of phenomena, which have no prior analogue, call for careful examinations of the mechanism of the QCP in the monolayer. Our experiments open a new avenue for studying unconventional QPTs and quantum critical matter.

Main Text

Monolayer WTe₂ is an excellent system for investigating the 2D superconducting QPT in a clean crystalline material with minimal disorder. Distinct from all previous systems studied experimentally, the insulating state of the monolayer is a QSHI⁴⁻⁶, where recent experiments and theories have shown evidence for an excitonic insulator phase at its charge neutrality point⁹⁻¹³. With electrostatic gating, superconductivity occurs in this 2D crystal above a very low critical carrier density^{7,8}, on the order of 10¹² cm⁻². Existing theories suggest that its pairing mechanism could be topological¹⁴ or spin-triplet¹⁵. Models investigating exotic phase transitions between a

QSHI and a superconductor exist^{16–18}. The nature of the low-density superconductivity and the intriguing superconductor-to-QSHI quantum transition in monolayer WTe₂ is currently unknown.

Vortex Nernst effect in the monolayer

We examine the superconducting QPT in monolayer WTe₂ by measuring the Nernst effect. The Nernst experiment detects a transverse voltage in a material placed in a perpendicular magnetic field (B) when a thermal gradient is applied in the longitudinal direction (Fig. 1a). In the case of a type-II superconductor, a magnetic field generates vortices that carry quantized flux and entropy in the superfluid. A temperature gradient ($-\nabla T$) can then drive a flow of vortices, producing phase slippage that engenders a transverse electric field (E) due to the Josephson relation. Since its observation in cuprates^{19,20} above the critical temperature (T_c), the Nernst effect has been widely observed in various superconductors²¹. As a sensitive probe to vortices and superconducting fluctuations, it reveals critical information hidden from electrical transport.

To detect the monolayer Nernst effect, we employ the geometry shown in Fig. 1a. The monolayer WTe₂ is fully encapsulated between graphite/hexagonal boron nitride (hBN) stacks to avoid degradation and enable gate-dependent studies (see Methods and Extended Data Fig. 1). The carrier density in the monolayer is modified by gate voltages applied to the top (V_{tg}) and bottom $(V_{\rm bg})$ graphite layers. The gate-induced carrier density is $n_{\rm g} \equiv \varepsilon_{\rm r} \varepsilon_0 (V_{\rm tg}/d_{\rm tg} + V_{\rm bg}/d_{\rm bg})/e$, where $d_{\rm tg}$ ($d_{\rm bg}$), ε_r , ε_0 , and e denotes, respectively, the thickness of top (bottom) hBN dielectric, its relative dielectric constant, vacuum permittivity, and elementary charge. Key to the Nernst experiments are the two microheaters fabricated next to the monolayer, each being a thin narrow metal stripe (~ 200 nm wide, ~ 8 nm thick, and ~ 1 k Ω resistance). We employ a dual-heater measurement scheme²²⁻²⁵, in which a low-frequency ($\omega \sim 13$ Hz) alternating current is applied to the two microheaters, with a 90° phase shift between them, to produce an alternating ∇T with minimal perturbation to the sample temperature (T). The Nernst voltage drop (V_N) across the two probes is detected at the frequency of 2\omega. Unlike in previous thermoelectric measurements on 2D materials where the heater is typically located on the SiO₂/Si substrate^{26–28}, here we fabricate the heaters directly inside the van der Waals stack. This method, which produces a finite ∇T with minimal heater power (P_h) (see Methods and Extended Data Figs. 2-4), enables Nernst measurements at millikelyin temperatures. Our approach can be universally applied to study the thermoelectricity of various 2D crystals and moiré materials.

Figure 1b depicts the electronic phase diagram of the monolayer, based on four-probe resistance (R_{xx}) taken on the same device (device 1) (Extended Data Fig. 5). Consistent with previous reports^{7,8}, it clearly shows both the superconducting and QSHI states with a critical carrier density, $n_{c,R} \sim 6.3 \times 10^{12}$ cm⁻², at which dR_{xx}/dT switches its sign. We characterize this gate-tuned 2D superconductor by the Berezinskii–Kosterlitz–Thouless (BKT) transition temperature (T_{BKT}), at which thermal fluctuations unbind vortex-antivortex pairs and produce a finite resistance. For each n_g well above $n_{c,R}$, we extract the corresponding T_{BKT} from its I-V characteristics following the usual procedure²⁹ (Extended Data Fig. 6). T_{BKT} , represented by the white dots in Fig. 1b, decreases monotonically with decreasing n_g and vanishes at a density slightly higher than $n_{c,R}$, signifying the n_g -tuned QPT.

We first present the Nernst data taken in the highly electron-doped regime ($n_{\rm g} \sim 2.3 \times 10^{13}$ cm²), where the highest $T_{\rm c}$ is observed. Figure 1c plots the Nernst signal ($V_{\rm N}$) together with $R_{\rm xx}$ as a function of B, where $V_{\rm N}$ clearly develops a peak at the field-induced transition to the normal state and vanishes near zero B (i.e., the vortex solid state) as well as at high B. With increasing T to high values, $V_{\rm N}$ disappears (Figs. 1d and e). The Nernst signal, which is antisymmetric with respect to B and coincides with the change in $R_{\rm xx}$, directly probes the motion of vortices in the vortex liquid state^{20,21,30}. We further note that the absence of $V_{\rm N}$ at high B and high T implies that the quasiparticle contributions to the Nernst signal are negligible in our measurements.

Large quantum fluctuations in the underdoped regime

Our key results are shown in Fig. 2a, where the Nernst signal is recorded at $T \sim 45$ mK as a function of $n_{\rm g}$, which is continuously tuned across the superconductor-to-QSHI transition. We discuss important findings near the $n_{\rm g}$ -tuned QPT in three regimes. The first one is the large Nernst signal observed in the underdoped regime at unexpectedly high B (labeled as "I" in Fig. 2a). In Fig. 2b, we present $R_{\rm xx}$ map measured under the same condition, where the black dotted line represents $B_{\rm R,90\%}$, at which $R_{\rm xx}$ drops to 90% of its saturated value at high B (Extended Data Fig. 5). The same dotted line is also plotted in Fig. 2a. Substantial $V_{\rm N}$ is observed in regime I, well above $B_{\rm R,90\%}$, despite that the $R_{\rm xx}$ data appears to suggest a normal resistive state with no hint of superconductivity. The Nernst data implies that there is a critical field, $B_{\rm c,N}$, above which $V_{\rm N}$ vanishes (the white dashed line in Fig. 2c). Figures 2c & d highlight the gate dependence of $B_{\rm c,N}$. In contrast to $B_{\rm R,90\%}$, $B_{\rm c,N}$ increases rapidly with decreasing $n_{\rm g}$ to the critical doping, where $B_{\rm c,N}$, at least ~ 500 mT, is more than ten times higher than the corresponding $B_{\rm R,90\%}$. Fig. 2e highlights the heater-power effect on $V_{\rm N}$. The implications of these observations will be further discussed below.

The prominent Nernst signal in the underdoped regime is enhanced at the lowest T. Figure 2f plots the T-dependent V_N , together with R_{xx} , at $n_g \sim 7.0 \times 10^{12}$ cm⁻². At this doping, the zero-field R_{xx} displays only a slight drop below ~ 200 mK but doesn't reach zero. At a B field of 150 mT, this low-T drop is completely suppressed, and an upturn is instead observed. Surprisingly, V_N at this B field remains substantial and survives to temperatures as high as ~ 700 mK (Fig. 2f), where traces of superconductivity in R_{xx} vanish at all dopings in this device (Fig. 1b). The Nernst signal above T_c was first observed in cuprates, indicating vortex-like excitations in the pseudogap regime 19,20 . Our observation here occurs in the quantum regime. Figure 2f shows that V_N increases strongly with decreasing T. By extrapolation, the Nernst signal is finite in the limit of zero kelvin. It thus arises from quantum fluctuations, instead of thermal fluctuations.

Giant Nernst effect at the QCP and its sudden disappearance

Remarkably, Fig. 2a clearly reveals a continuous evolution from the vortex liquid regime at high electron doping to the strongly quantum fluctuating regime near the n_g -tuned QPT in a single device. Sharply located at the QPT (labeled as "II" in Fig. 2a), the quantum fluctuations produce a giant Nernst signal near zero B, which is another key finding. In Fig. 3a, we carefully examine this regime by plotting V_N under very small B. One immediately observes that the Nernst signal is extremely sensitive to the QPT, i.e., a slight detuning of n_g away from $n_{\text{max}} \sim 7.2 \times 10^{12} \text{ cm}^{-2}$, where V_N is maximized, completely suppresses the signal on both sides. To demonstrate that this signal reflects the zero-B property of the QCP, we plot V_N/B in Fig. 3b (only the positive-B side is shown),

which may be interpreted as the mobility of the vortices and shows a strong enhancement when B is reduced to near zero. Figure 3c further plots V_N versus B curves at selected n_g , in which we confirm that the largest slope occurs at n_{max} near zero B. In Methods, we estimate ∇T to be ~ 5.3 mK/ μ m, based on which we obtain the corresponding Nernst coefficient, $v = (dE/dB)/\nabla T|_{B=0}$, to be $\sim 4,100 \,\mu\text{V/KT}$, among the largest values measured in all materials. As a comparison, this giant Nernst coefficient is at least one order of magnitude higher than the typical v measured in other superconductors 20,21,30,31 . This large Nernst response near zero B indicates the proliferation of vortices and antivortices when the doping is reduced to the critical value.

The large Nernst signal abruptly disappears right below $n_{c,R} \sim 6.3 \times 10^{12}$ cm⁻² (labeled as "III" in Fig. 2a, and also in Figs. 3a & b). While the vanishing of V_N above n_{max} is expected in the vortex solid state, its sudden disappearance right below $n_{c,R}$ is a surprise. As a comparison, previous studies in disordered superconducting films have reported substantial Nernst signal deep inside the insulating phase after the transition³¹, in clear contrast to the monolayer WTe₂. Note that the noisy data that appears below $\sim 3.4 \times 10^{12}$ cm⁻² in Figs. 2a & 3a is not antisymmetric in B and hence not a Nernst signal (they likely arise due to bad contacts in the more insulating state). The absence of a Nernst signal in regime III is intrinsic, rather than a consequence of resolution limitations in the experiments. This can be seen in Fig. 2e, which reveals a clear contrast in the heater-power dependence of V_N between regimes III and I', and demonstrates that V_N is invariably absent in regime III despite the 10-fold increase in heater power. This is true at all magnetic fields up to 500 mT (see Figs. 2c & d). Regime III is also anomalous in electrical transport. Figure 3d plots R_{xx} , where n_{max} and $n_{\text{c,R}}$ are both indicated by the red dashed lines. One finds that while R_{xx} displays a dramatic T dependence on the superconducting side, its value in regime III, on the order of $\sim k\Omega$ at millikelvin, displays little changes with T. This indicates that a metallic-like state resides right below $n_{c,R}$, before the QSHI/excitonic insulator^{6,9,10} is fully developed. The sudden disappearance of $V_{\rm N}$ implies the complete absence of superconducting fluctuations in the metallic-like state directly abutting the QPT. The extreme asymmetry in V_N is our key result.

These highly reproducible findings (see Extended Data Fig. 7 for the data taken on device 2) highlight the intriguing nature of the n_g -tuned QPT in monolayer WTe₂. Fig. 4a sketches the phase diagrams based on our observations. To reinforce that the Nernst signal reflects the superconducting quantum fluctuations, in Fig. 4b, we plot the T-dependent V_N , taken at a fixed small B (2 mT). The amplitude of the signal increases rapidly when T is lowered, suggesting that the Nernst coefficient (ν) attains its maximum at zero kelvin. The corresponding n_{max} shifts its values at different T, which traces precisely the T_{BKT} determined from the transport measurement (the same as Fig. 1b). In the canonical phase diagram of a QPT, sketched in the inset of Fig. 4a lower panel, the BKT transition traces down to the QCP at absolute zero. The Nernst signal hence directly detects the superconducting QCP in the monolayer. Clearly, quantum fluctuations at the QCP produce the dramatic Nernst signal at the lowest T.

Discussion

This series of unusual phenomena observed here in monolayer WTe₂ has no prior analogue in research on 2D superconducting transitions and challenges the conventional wisdom on QPTs. The standard Landau-Ginzburg-Wilson (LGW) theory³² describes a continuous transition between

an ordered state and a "disordered" state. The order parameter fluctuations are expected to be stronger on the "disordered" side reflecting the suppression of phase fluctuations on the ordered side. In a superconducting transition, a pronounced fluctuation tail penetrating into the normal state is expected and may be further enhanced in the presence of a vortex liquid state above the transition, as widely seen in cuprates²⁰. Such conventional expectations of stronger fluctuations on the non-superconducting side (Fig. 4c upper panel) are general, independent of the tuning parameter used for inducing the transition.

In our experiments, we observed three types of superconducting phase transitions in a single device (see Fig. 4a): (a) the T-tuned transition; (b) the B-tuned transition; and (c) the n_g -tuned transition. Indeed, both (a) and (b) follow the above conventional expectations, i.e., pronounced Nernst signals are seen in the normal states (see, e.g., Fig. 2f for the T-tuned transition and Figs. 2a & c for the B-tuned transition). However, the transition of (c), the n_g -tuned QPT, is strikingly opposite to the conventional expectation (Fig. 4c lower panel). The sudden disappearance of the Nernst signal in the normal state below the critical doping n_c (regime III in Fig. 2a) is not anticipated at all in the LGW picture. We conclude that the n_g -tuned superconducting QCP in monolayer WTe₂ is unconventional.

We further summarize the key experimental features related to this unconventional QCP in Fig. 4d. In the regime $n_g > n_c$, $B_{c,N}$ provides a measure of the pairing strength in the superconducting state. The increase of $B_{\rm c,N}$ implies that the pairing strength increases monotonically as $n_{\rm g} \to n_{\rm c}^+$ (Fig. 4d upper panel), an unexpected behavior. Paradoxically, in spite of the increasing pairing strength, $V_{\rm N}$ vanishes abruptly once $n_{\rm g}$ is decreased below $n_{\rm c}$. One possible way to explain the sudden disappearance of V_N is to assume that a new ordered phase emerges in regime III $(n_g \le n_c)$. This is suggested by the fluctuations in the following two limits. In the limit of $B \to 0$ and $T \to 0$ (Fig. 4d middle panel), the giant Nernst response observed at n_c separates two distinct phases with no detectable fluctuations on either side. On the right side, this is understood because the pairing leads to an ordered superconducting state. It is however challenging to explain the absence of fluctuations on the left side if it is treated as a usual metallic-like state. As a comparison, in the limit of large B and $T \to 0$ (Fig. 4d lower panel), the right side is now in a normal metal state (above $B_{c,N}$). Reducing $n_g \to n_c^+$, strong Nernst signal occurs and signifies the fluctuations, with a long tail appearing on the right metallic side. This is in sharp contrast to the sudden disappearance of $V_{\rm N}$ on the left side, even though it displays a similar metallic-like resistivity. The highly asymmetric fluctuations (the lower panel) again seem to suggest a transition from the normal metallic phase (above n_c) to an ordered phase (below n_c) that does not superconduct. In Extended Data Fig. 8, we present experimental evidence for ruling out a first-order transition. Our experiments, without relying on any model, raise an intriguing question of whether a novel continuous QPT that directly connects two distinct ordered phases is realized here in the monolayer. Note that the metallic phase below n_c (regime III) arises from doping electrons into the excitonic QSHI, which might be an important clue for uncovering its nature.

The unconventional quantum fluctuations detected in monolayer WTe₂ highlight again the unusual electronic properties of this material, in which deep connections between its topological and correlated physics remain to be resolved. Several other 2D systems have also shown interesting quantum criticality^{33–36}, while the physics is distinct from the case reported here. Our experiments

show that, in general, fluctuations in the vicinity of a QCP provide a powerful probe to the nature of a QPT.

References

- 1. Goldman, A. M. & Marković, N. Superconductor-Insulator Transitions in the Two-Dimensional Limit. *Phys Today* **51**, 39–44 (1998).
- 2. Kapitulnik, A., Kivelson, S. A. & Spivak, B. Colloquium: Anomalous metals: Failed superconductors. *Rev. Mod. Phys.* **91**, 011002 (2019).
- 3. Lin, Y.-H., Nelson, J. & Goldman, A. M. Superconductivity of very thin films: The superconductor-insulator transition. *Phys. C Supercond. Appl.* **514**, 130–141 (2015).
- 4. Qian, X., Liu, J., Fu, L. & Li, J. Quantum spin Hall effect in two-dimensional transition metal dichalcogenides. *Science* **346**, 1344–1347 (2014).
- 5. Fei, Z. et al. Edge conduction in monolayer WTe₂. Nat. Phys. 13, 677–682 (2017).
- 6. Wu, S. *et al.* Observation of the quantum spin Hall effect up to 100 kelvin in a monolayer crystal. *Science* **359**, 76–79 (2018).
- 7. Fatemi, V. *et al.* Electrically tunable low-density superconductivity in a monolayer topological insulator. *Science* **362**, eaar4642 (2018).
- 8. Sajadi, E. *et al.* Gate-induced superconductivity in a monolayer topological insulator. *Science* **362**, eaar4426 (2018).
- 9. Wang, P. et al. Landau quantization and highly mobile fermions in an insulator. *Nature* **589**, 225–229 (2021).
- 10. Jia, Y. et al. Evidence for a monolayer excitonic insulator. Nat. Phys. 18, 87–93 (2022).
- 11. Sun, B. *et al.* Evidence for equilibrium exciton condensation in monolayer WTe₂. *Nat. Phys.* **18**, 94–99 (2022).
- 12. Lee, P. A. Quantum oscillations in the activated conductivity in excitonic insulators: Possible application to monolayer WTe₂. *Phys. Rev. B.* **103**, L041101 (2021).
- 13. Kwan, Y. H., Devakul, T., Sondhi, S. L. & Parameswaran, S. A. Theory of competing excitonic orders in insulating WTe₂ monolayers. *Phys. Rev. B.* **104**, 125133 (2021).
- 14. Hsu, Y.-T., Cole, W. S., Zhang, R.-X. & Sau, J. D. Inversion-Protected Higher-Order Topological Superconductivity in Monolayer WTe₂. *Phys. Rev. Lett.* **125**, 097001 (2020).
- 15. Crépel, V. & Fu, L. Spin-triplet superconductivity from excitonic effect in doped insulators. *Proc. Natl. Acad. Sci.* **119**, e2117735119 (2022).
- 16. Grover, T. & Senthil, T. Topological Spin Hall States, Charged Skyrmions, and Superconductivity in Two Dimensions. *Phys. Rev. Lett.* **100**, 156804 (2008).
- 17. Liu, Y. *et al.* Superconductivity from the condensation of topological defects in a quantum spin-Hall insulator. *Nat. Commun.* **10**, 2658 (2019).
- 18. Wang, Z. *et al.* Doping-Induced Quantum Spin Hall Insulator to Superconductor Transition. *Phys. Rev. Lett.* **126**, 205701 (2021).
- 19. Xu, Z. A., Ong, N. P., Wang, Y., Kakeshita, T. & Uchida, S. Vortex-like excitations and the onset of superconducting phase fluctuation in underdoped La_{2-x}Sr_xCuO₄. *Nature* **406**, 486–488 (2000).

- 20. Wang, Y., Li, L. & Ong, N. P. Nernst effect in high-T_c superconductors. *Phys. Rev. B.* **73**, 024510 (2006).
- 21. Rischau, C. W. *et al.* Universal Bound to the Amplitude of the Vortex Nernst Signal in Superconductors. *Phys. Rev. Lett.* **126**, 077001 (2021).
- 22. Aubin, M., Ghamlouch, H. & Fournier, P. Measurement of the Seebeck coefficient by an ac technique: Application to high-temperature superconductors. *Rev. Sci. Instrum.* **64**, 2938–2941 (1993).
- 23. Resel, R. *et al.* Thermopower measurements in magnetic fields up to 17 tesla using the toggled heating method. *Rev. Sci. Instrum.* **67**, 1970–1975 (1996).
- 24. Choi, E. S., Brooks, J. S., Qualls, J. S. & Song, Y. S. Low-frequency method for magnetothermopower and Nernst effect measurements on single crystal samples at low temperatures and high magnetic fields. *Rev. Sci. Instrum.* **72**, 2392–2397 (2001).
- 25. Li, X.-Q., Li, Z.-L., Zhao, J.-J. & Wu, X.-S. Electrical and thermoelectric study of two-dimensional crystal of NbSe₂. *Chinese Phys. B.* **29**, 087402 (2020).
- 26. Zuev, Y. M., Chang, W. & Kim, P. Thermoelectric and Magnetothermoelectric Transport Measurements of Graphene. *Phys. Rev. Lett.* **102**, 096807 (2009).
- 27. Checkelsky, J. G. & Ong, N. P. Thermopower and Nernst effect in graphene in a magnetic field. *Phys. Rev. B.* **80**, 081413(R) (2009).
- 28. Wei, P., Bao, W., Pu, Y., Lau, C. N. & Shi, J. Anomalous Thermoelectric Transport of Dirac Particles in Graphene. *Phys. Rev. Lett.* **102**, 166808 (2008).
- 29. Saito, Y., Nojima, T. & Iwasa, Y. Highly crystalline 2D superconductors. *Nat. Rev. Mater.* **2**, 16094 (2016).
- 30. Ienaga, K., Hayashi, T., Tamoto, Y., Kaneko, S. & Okuma, S. Quantum Criticality inside the Anomalous Metallic State of a Disordered Superconducting Thin Film. *Phys. Rev. Lett.* **125**, 257001 (2020).
- 31. Roy, A., Shimshoni, E. & Frydman, A. Quantum Criticality at the Superconductor-Insulator Transition Probed by the Nernst Effect. *Phys. Rev. Lett.* **121**, 047003 (2018).
- 32. Sachdev, S. Quantum Phase Transitions, 2nd ed. (Cambridge University Press, Cambridge, England, 2011).
- 33. Yang, C. *et al.* Intermediate bosonic metallic state in the superconductor-insulator transition. *Science* **366**, 1505–1509 (2019).
- 34. Ghiotto, A. *et al.* Quantum criticality in twisted transition metal dichalcogenides. *Nature* **597**, 345–349 (2021).
- 35. Li, Q. *et al.* Tunable quantum criticalities in an isospin extended Hubbard model simulator. *Nature* **609**, 479–484 (2022).
- 36. Jaoui, A. *et al.* Quantum critical behaviour in magic-angle twisted bilayer graphene. *Nat. Phys.* **18**, 633–638 (2022).
- 37. Wang, P. *et al.* Piezo-driven sample rotation system with ultra-low electron temperature. *Rev. Sci. Instrum.* **90**, 023905 (2019).

Acknowledgments

We acknowledge helpful discussions with Z. Bi, T. Grover, F. D. M. Haldane, D. Huse, B. Lian, S. Ryu, S. Sondhi, A. Vishwanath, A. Yazdani, and Y. Zhang. We especially thank L. Pfeiffer and M. Shayegen for their GaAs sample, which was used for calibrating the electron temperature

of our dilution refrigerator. This work is mainly supported by ONR through a Young Investigator Award (N00014-21-1-2804) to S.W. Measurement systems and data collection are partially supported by NSF through a CAREER award (DMR-1942942) to S.W. Data analysis is partially supported by AFOSR Young Investigator program (FA9550-23-1-0140) to S.W. N.P.O. is supported by the U.S. Department of Energy (DE-SC0017863). S.W. and L.M.S. acknowledge support from the Eric and Wendy Schmidt Transformative Technology Fund at Princeton. Materials synthesis and device fabrication are partially supported by the Materials Research Science and Engineering Center (MRSEC) program of the National Science Foundation (DMR-2011750) through support to R.J.C., L.M.S., N.P.O., and S.W. T.S. acknowledges support from the Princeton Physics Dicke Fellowship program. A.J.U. acknowledges support from the Rothschild Foundation and the Zuckerman Foundation. K.W. and T.T. acknowledge support from the JSPS KAKENHI (Grant Numbers 19H05790, 20H00354, and 21H05233). L.M.S. and N.P.O. acknowledge support from the Gordon and Betty Moore Foundation through Grants GBMF9064 and GBMF9466, respectively. L.M.S is also supported by the David and Lucile Packard Foundation and the Sloan Foundation.

Author contributions

S.W. designed the project. T.S. fabricated the devices and performed measurements, assisted by Y.J., Y.T., G.Y., P.W., A.J.U., and M.O. G.Y. and P.W. built the dilution refrigerator measurement system. T.S., S.W., and N.P.O. analyzed the data. R.S., L.M.S., X.G., and R.J.C. grew and characterized bulk WTe₂ crystals. K.W. and T.T. provided hBN crystals. S.W., T.S., and N.P.O. interpreted the results and wrote the paper with input from all authors.

Competing interests

The authors declare that they have no competing interests.

Data availability

All data needed to evaluate the conclusions in the paper are presented in the paper. Additional data related to this paper are available from the corresponding author upon reasonable request.

Fig. 1

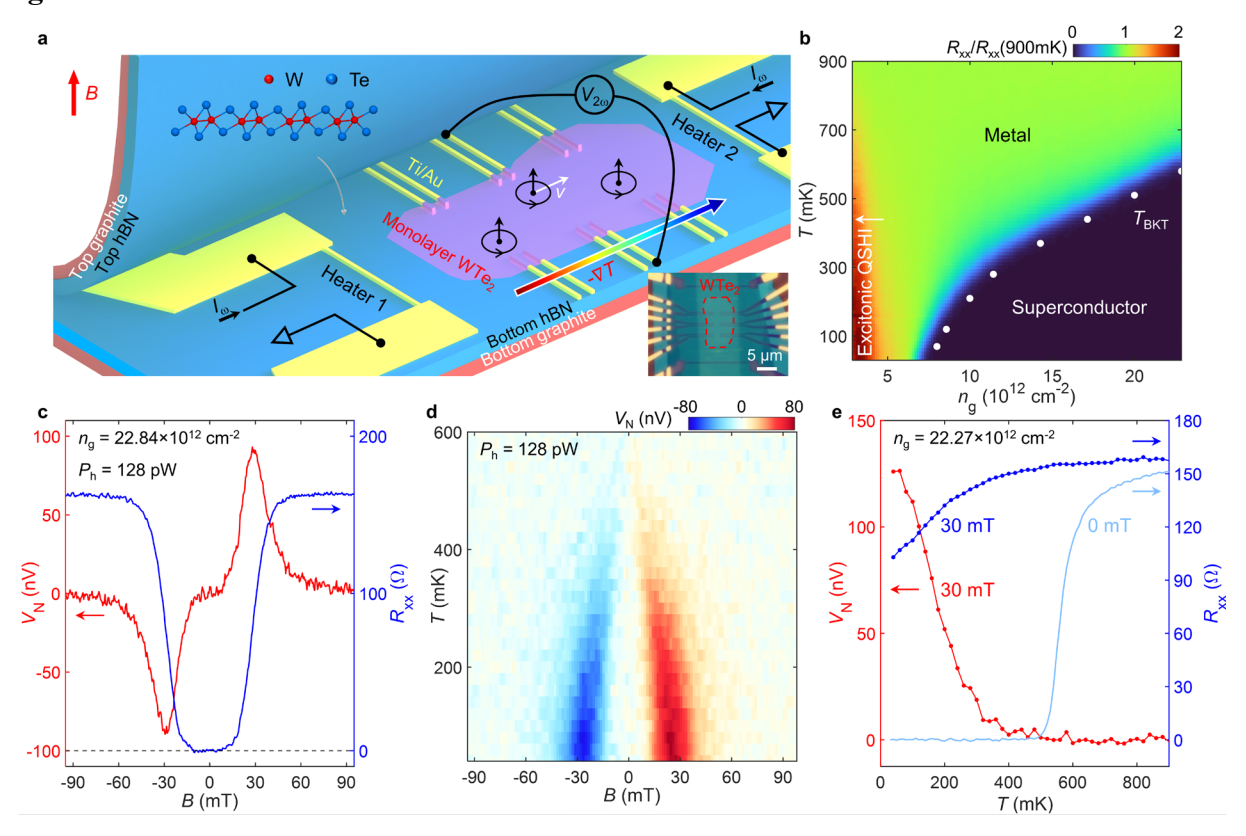


Fig. 1 | Vortex Nernst effect and electronic phase diagram of monolayer WTe₂. a, Cartoon illustration of the device structure for measuring Nernst signal. Current is applied to the two microheaters to produce a temperature gradient on the monolayer WTe₂. The inset shows the optical microscope image of device 1. The monolayer WTe₂ flake is outlined in red. b, Four-probe resistance as a function of n_g and T, measured on the same device. For each n_g , R_{xx} is normalized to its value at 900 mK to highlight its temperature dependence (also see Extended Data Fig. 5). The white dots represent T_{BKT} . c, Nernst signal (red) and R_{xx} (blue) as a function of magnetic field (B) for $n_g = 22.84 \times 10^{12}$ cm⁻². The dual-heater power (P_h) is 128 pW. d, B_h -dependence of V_N as a function of T for the same n_g . e, T-dependence of V_N (red) and R_{xx} (blue) measured at 30 mT for $n_g = 22.27 \times 10^{12}$ cm⁻². The zero-field R_{xx} is shown as a reference (light blue).

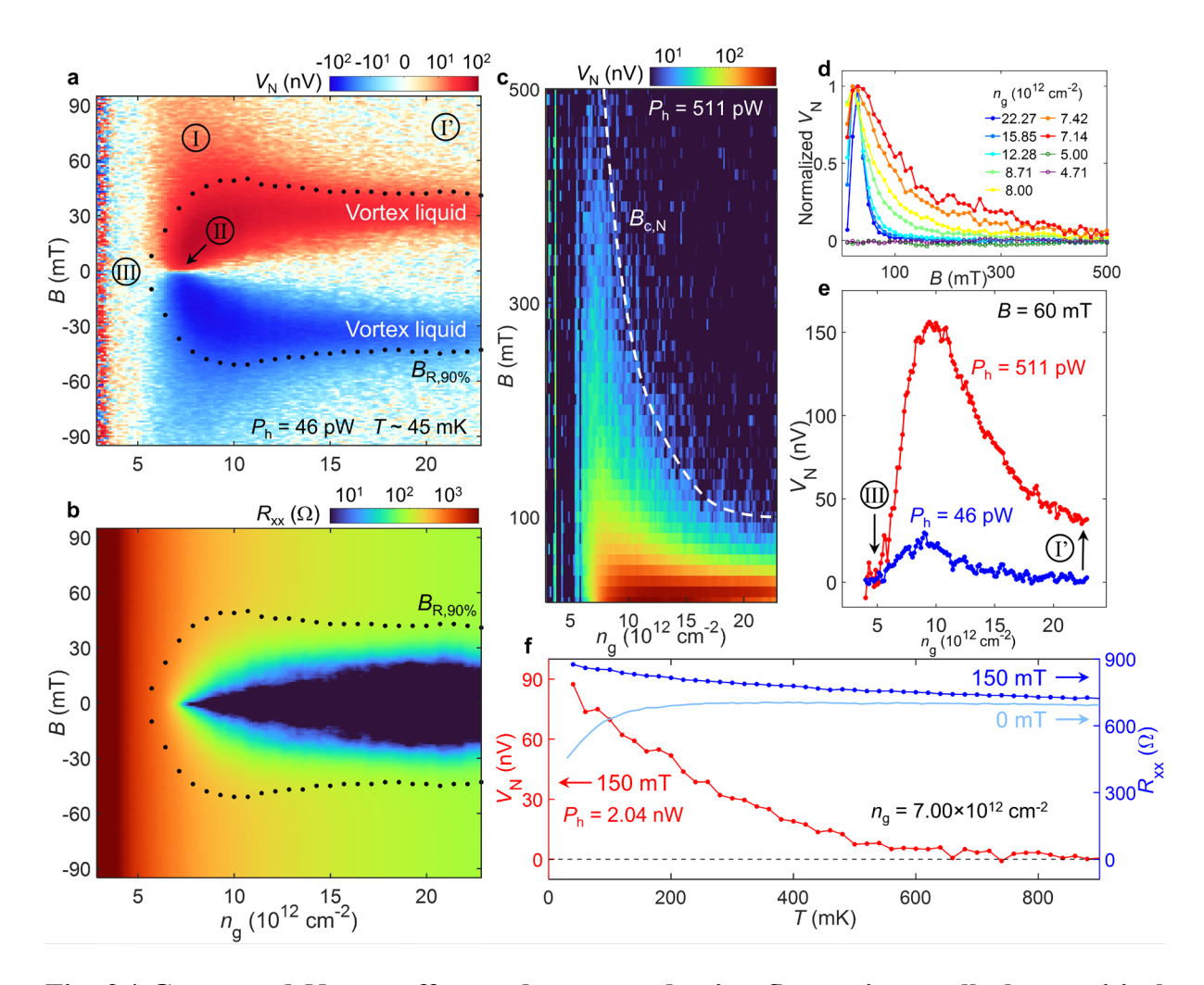


Fig. 2 | Gate-tuned Nernst effect and superconducting fluctuations well above critical magnetic field and critical temperature. a, Nernst signal as a function of n_g and B. Three different regimes of interest are labeled as I, II, III, respectively. b, R_{xx} as a function of n_g and B measured under the same condition as **a**. The black dotted line represents $B_{R,90\%}$, at which R_{xx} drops to 90% of its saturated value at high B. c, Nernst signal measured up to high B, with a higher power ($P_h = 511 \text{ pW}$). The white dashed line indicates the critical field, $B_{c,N}$, above which V_N vanishes. d, n_g -dependence of the Nernst signal versus B. V_N is normalized to its peak value. e, Heater-power effect on the Nernst signal. The data are horizontal line cuts of **a** and **c**, respectively, at B = 60 mT. f, T-dependence of V_N (red) and R_{xx} (blue) measured at 150 mT for a selected low density near the QPT ($n_g = 7.00 \times 10^{12} \text{ cm}^{-2}$). The zero-field R_{xx} is shown as a reference (light blue).



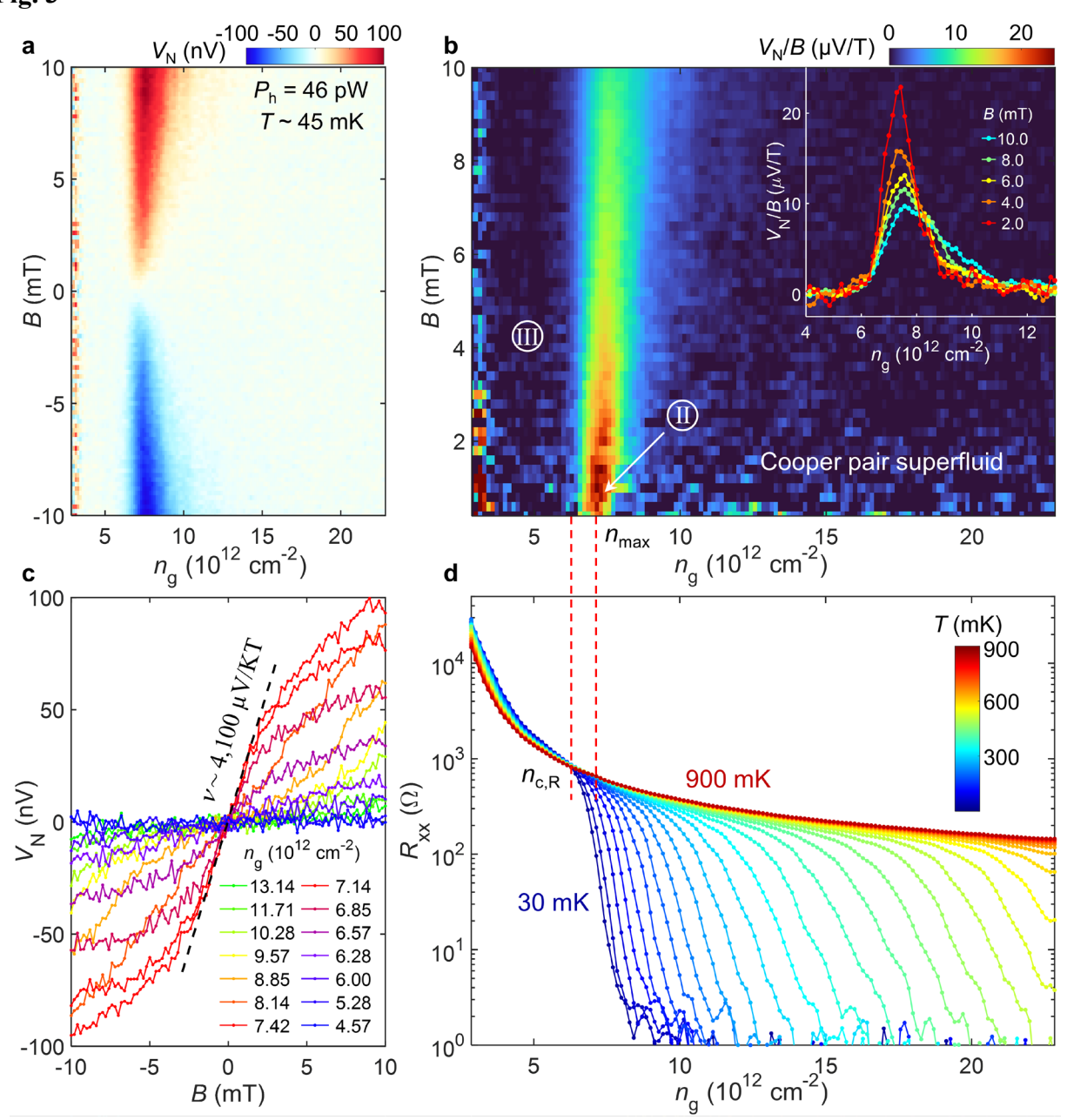


Fig. 3 | Giant Nernst effect at the QCP and its sudden disappearance. a, Nernst signal as a function of n_g under very small B. b, V_N/B as a function of n_g and B, calculated from a. Only the positive-B side is shown. Inset displays selected line cuts of the same data. c, V_N versus B curves at selected n_g . The dashed line extracts the largest slope, which occurs at n_{max} near zero B. The estimated v is indicated. d, T-dependence of R_{xx} versus n_g . The two red dashed lines indicate $n_{\text{c,R}}$ and n_{max} , respectively.

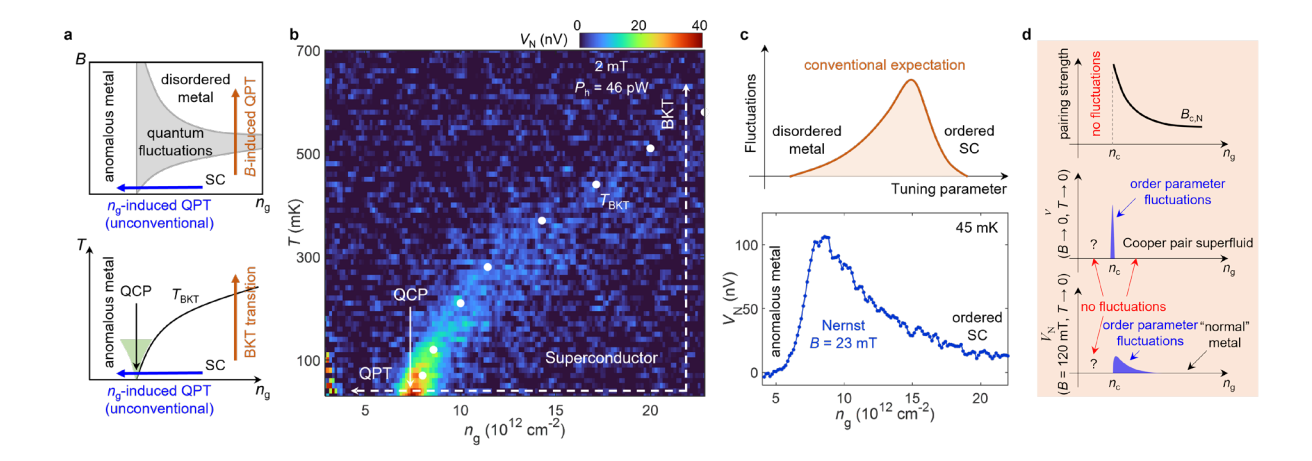


Fig. 4 | **QPT and anomalous quantum fluctuations detected by Nernst effect. a**, Schematic phase diagrams showing three types of superconducting phase transitions observed in our device. **b**, Nernst signal as a function of n_g and T. The white dots represent $T_{\rm BKT}$. The inset sketches the typical phase diagram of a QPT, where the tuning parameter (g) is realized by n_g in our case. **c**, Contrast between the Nernst signal (lower panel, data extracted from Fig. 2a) and the expected fluctuations from the conventional LGW theory (upper panel). **d**, Illustrations of some key findings summarized from Figs. 2 and 3.